Comparison of the Stability of the Atlantic Thermohaline Circulation in Two Coupled Atmosphere–Ocean General Circulation Models

JIANJUN YIN*

Program in Atmospheric and Oceanic Sciences, Princeton University, Princeton, New Jersey

RONALD J. STOUFFER

NOAA/Geophysical Fluid Dynamics Laboratory, Princeton, New Jersey

(Manuscript received 4 May 2006, in final form 11 January 2007)

ABSTRACT

Two coupled atmosphere–ocean general circulation models developed at GFDL show differing stability properties of the Atlantic thermohaline circulation (THC) in the Coupled Model Intercomparison Project/Paleoclimate Modeling Intercomparison Project (CMIP/PMIP) coordinated "water-hosing" experiment. In contrast to the R30 model in which the "off" state of the THC is stable, it is unstable in the CM2.1. This discrepancy has also been found among other climate models. Here a comprehensive analysis is performed to investigate the causes for the differing behaviors of the THC. In agreement with previous work, it is found that the different stability of the THC is closely related to the simulation of a reversed thermohaline circulation (RTHC) and the atmospheric feedback. After the shutdown of the THC, the RTHC is well developed and stable in R30. It transports freshwater into the subtropical North Atlantic, preventing the recovery of the salinity and stabilizing the off mode of the THC. The flux adjustment is a large term in the water budget of the Atlantic Ocean. In contrast, the RTHC is weak and unstable in CM2.1. The atmospheric feedback associated with the southward shift of the Atlantic ITCZ is much more significant. The oceanic freshwater convergence into the subtropical North Atlantic cannot completely compensate for the evaporation, leading to the recovery of the THC in CM2.1. The rapid salinity recovery in the subtropical North Atlantic excites large-scale baroclinic eddies, which propagate northward into the Nordic seas and Irminger Sea. As the large-scale eddies reach the high latitudes of the North Atlantic, the oceanic deep convection restarts. The differences in the southward propagation of the salinity and temperature anomalies from the hosing perturbation region in R30 and CM2.1, and associated different development of a reversed meridional density gradient in the upper South Atlantic, are the cause of the differences in the behavior of the RTHC. The present study sheds light on important physical and dynamical processes in simulating the dynamical behavior of the THC.

1. Introduction

The hypothesis that the earth's climate system has multiple equilibria under the current climate forcing is supported by the bistability of the Atlantic thermohaline circulation (THC) found in climate models. The THC here refers to the giant meridional overturning circulation (MOC) in the Atlantic Ocean, with warm seawater flowing northward in the upper Atlantic and cold seawater flowing southward at depth (Wunsch 2002). The THC is closely related to the oceanic deep convection and the North Atlantic Deep Water (NADW) formation in the high latitudes of the North Atlantic. Many models suggest that, in addition to the current climate state with a vigorous THC (the "on" mode), a state without an active THC (the "off" mode) could be also stable under the same external forcing (Stommel 1961; Bryan 1986; Manabe and Stouffer 1988, 1999; Stocker and Wright 1991; Marotzke and Willebrand 1991; Weaver and Hughes 1994; Rahmstorf 1995). In response to global warming, the THC slows down during this century in most models (Manabe et al.

* Current affiliation: COAPS, The Florida State University, Tallahassee, Florida.

Corresponding author address: Jianjun Yin, Program in Atmospheric and Oceanic Sciences, Princeton University, P.O. Box CN710, Princeton, NJ 08544.
E-mail: Jianjun.Yin@noaa.gov

DOI: 10.1175/JCLI4256.1

1991; Cubasch et al. 2001; Gregory et al. 2005), with some studies indicating that significant change is possible if the CO_2 concentration continues to increase (Manabe and Stouffer 1994; Stocker and Schmittner 1997; Schlesinger et al. 2006). A recent ocean observational study indicates that the Atlantic MOC may have weakened by 30% during the past 50 years (Bryden et al. 2005), although this estimated change is very close to the error limits of the calculation and no temperature signal has been observed. Research suggests that, if the weakening of the THC goes beyond some critical point, the entire climate system can be switched into a different equilibrium and may not be easily returned to the current state unless another critical point can be passed (Rahmstorf 1995; Tziperman 1997).

A recent study under the framework of the Coupled Model Intercomparison Project (CMIP) and Paleoclimate Modeling Intercomparison Project (PMIP) has shown differing stability properties of the THC among climate models, ranging from the earth system models with intermediate complexity (EMICs) to the coupled atmosphere–ocean general circulation models (AOGCMs; Stouffer et al. 2006a). In particular, two fully coupled AOGCMs developed and used at the Geophysical Fluid Dynamics Laboratory (GFDL)—R30 and CM2.1—show distinctly different behavior of the THC to the external forcing. In response to a 1.0-Sv ($\text{Sv} \equiv 10^6\ \text{m}^3\ \text{s}^{-1}$) freshwater perturbation in the northern North Atlantic (the so-called water-hosing experiment; see section 2 for details about the experimental design), the THC shuts down and does not recover during the 200-yr period after the hosing is removed in R30 (Fig. 13 of Stouffer et al. 2006a). In contrast, it recovers rapidly in CM2.1 after the termination of the freshwater perturbation at the end of the 100th year. A similar recovery of the THC has also been found in other climate models (Schiller et al. 1997; Vellinga et al. 2002; Lohmann 2003). Comparing R30 and CM2.1 responses is of interest and importance. Given that the freshwater addition of 1.0 Sv represents a strong perturbation in a climatological perspective, the different behaviors of the THC suggest that the "off" state of the THC is a stable state in R30, while it is an unstable state in CM2.1 in the water-hosing experiment. A similar disagreement among models has also been found in another intercomparison study mainly focusing on the EMICs (Rahmstorf et al. 2005).

While the different results from R30 and CM2.1 seem to suggest different bistability of the THC under the present-day climate forcing, it should be noted that the term "bistability" is typically used when discussing the equilibrium response of the THC to external freshwater forcing and its hysteresis behavior (Rahmstorf et al. 2005). Here we study the transient THC response to a 100-yr 1.0-Sv freshwater input. So far, we do not know whether or not the results from transient runs are comparable to those from equilibrium runs in terms of the bistability of the THC. Compared to the latter, the former can be regarded as a zero effective freshwater perturbation experiment. The THC may have two stable states in both R30 and CM2.1 within some freshwater forcing regime if the external perturbation is applied indefinitely.

As a part of the ongoing work of the CMIP/PMIP coordinated water-hosing experiment, this paper explores potential reasons why the off THC state is stable in R30, but unstable in CM2.1 in response to a 100-yr 1.0-Sv freshwater input. By performing detailed and comprehensive comparison, we will identify the critical processes responsible for the different behaviors of the THC in these two AOGCMs. It is hoped that the present analyses shed light on the possible mechanisms that can explain the differences among the other models. But a robust conclusion cannot be drawn without a comprehensive Model Intercomparison Project (MIP) and associated analysis. This paper is organized as follows. Section 2 will describe the AOGCMs used by the present study and the experimental design. Section 3 will compare the 1.0-Sv water-hosing experiments from these two AOGCMs in detail. The processes responsible for the identified difference will be analyzed in section 4, followed by a discussion and conclusions section toward the end.

2. Model description and experimental design

The models used by the present study are GFDL R30 (R30 hereafter) and GFDL CM2.1 (CM2.1 hereafter). The R30 and CM2.1, as the previous and the latest generation of the climate models used at GFDL, bear significant differences both in their formulation and in the fidelity of the simulation of present-day climate. The atmospheric component of R30 is based on the spectral transform method with zonal truncation at wavenumber 30 (Delworth et al. 2002). The horizontal resolution is equivalent to 2.25° latitude by 3.75° longitude. There are 14 unevenly spaced levels in the vertical direction. Over land a simple "bucket" formulation is adopted to represent the surface hydrological processes. The ocean component of R30 is based on Modular Ocean Model version 1.1 (MOM1.1) (Pacanowski et al. 1991). The Boussinesq, rigid-lid, and hydrostatic approximations are made to solve the primitive equations of the ocean dynamics. The horizontal resolution of the oceanic model is 2.25° latitude by 1.875° longitude with 18 vertical levels. The subgrid mixing of momentum

TABLE 1. Model information for R30 and CM2.1.

	R30	CM2.1
Atmospheric model resolution	R30 (2.25° × 3.75°), L14	2° × 2.5°, L24, finite volume dynamical core
Oceanic model resolution	MOM1.1, 2.25° × 1.9°, L18	MOM4, 1° × 1° with enhanced resolution at Tropics (⅓° at equator), L50, tripolar
Ocean surface	Rigid-lid approximation	Free surface
Land model	Standard bucket scheme	Complex land surface scheme
Sea ice model	A relatively simple sea ice model where the sea ice is advected by the top-layer ocean velocity	Thermodynamic–dynamic, multiple ice categories
Surface water flux method	Virtual salt flux	Freshwater flux
Flux adjustment	Heat, water	None
CO_2 (ppmv)	360	286
Solar constant (W m^{-2})	1365	1365
Oceanic diffusivity (m^2 s^{-1})	Background horizontal: 4×10^2, isopycnal: $1.9 \times 10^3 \sim 1 \times 10^3$, horizontal: 1.2×10^5, vertical: $0.3 \sim 1.0 \times 10^{-4}$	Gent–McWilliams scheme
Reference	Delworth et al. (2002)	Delworth et al. (2006); Gnanadesikan et al. (2006); Wittenberg et al. (2006); Stouffer et al. (2006); Griffies et al. (2006)

and tracers are parameterized using the schemes proposed by Bryan and Lewis (1979) and Cox (1987). In addition, a secondary "background" mixing is also implemented in the horizontal and vertical directions. Here R30 uses a relatively simple sea ice model where the sea ice is advected by the top-layer ocean velocity (Bryan 1969) and employs heat and water flux adjustment at the ocean surface to compensate the climate drift.

The horizontal resolution of the atmospheric model and land model of CM2.1 is 2° latitude by 2.5° longitude. The atmospheric model has 24 vertical levels. It employs a finite volume dynamical core (Lin 2004) and 1860 radiative forcing condition. The oceanic model is based on the GFDL MOM4 code (Griffies et al. 2003), which uses a horizontal tripolar grid to avoid the North Pole singularity (Murray 1996). The horizontal resolution is 1° in latitude and longitude with enhanced resolution in the meridional direction at the Tropics, so the meridional resolution is ⅓° near the equator. There are 50 vertical levels with 22 levels in the top 220 m. The detailed physical parameterization of the oceanic model can be found in Griffies et al. (2003). A dynamical–thermodynamical sea ice model with the elastic–viscous–plastic technique to calculate ice internal stresses is used to predict the sea ice. The component models are coupled together by a coupler that calculates and passes fluxes at the component model interfaces. Compared with R30, CM2.1 has been developed from entirely new codes and algorithms. In addition, it uses a finer grid resolution and more sophisticated physical parameterizations and does not need flux adjustments to maintain a stable control climate. The details of the model configurations, coupling procedure, and performance can be found in Delworth et al. (2006), Gnanadesikan et al. (2006), Wittenberg et al. (2006), Stouffer et al. (2006b), and Griffies et al. (2006). Table 1 gives a brief comparison of R30 and CM2.1.

In addition to the model formulation, the values of the CO_2 concentration are also different between the two models (Table 1). During the integrations presented here, the CO_2 concentrations are held constant so that the differences in the response are due to the imposed freshwater flux perturbations rather than any changes in the radiative forcing. Potentially, the use of different values for the CO_2 concentration could cause differences in the control climates. However, the use of flux adjustments in the R30 and the relatively small climate drifts found in the CM2.1 model results allow the control integrations of the two models to be similar to each other and to observations (Figs. 1–3). In comparison with the observations, the control climates in both models are realistic. The larger error in the control run of CM2.1 is climate drift, resulting from the imperfections found in the model and not using flux adjustments. The detailed analysis of the model bias can be found in previous model documentations (Delworth et al. 2002, 2006). Given the large imposed freshwater flux perturbation described below, any differences in the response between the models are likely not the result of the relatively small differences in the control climates.

In the water-hosing experiment, a freshwater perturbation of 1.0 Sv is input uniformly into 50°–70°N of the North Atlantic for 100 years. The freshwater flux of 1.0 Sv is approximately equal to the total river runoff over the world and is sufficiently large to shut down the

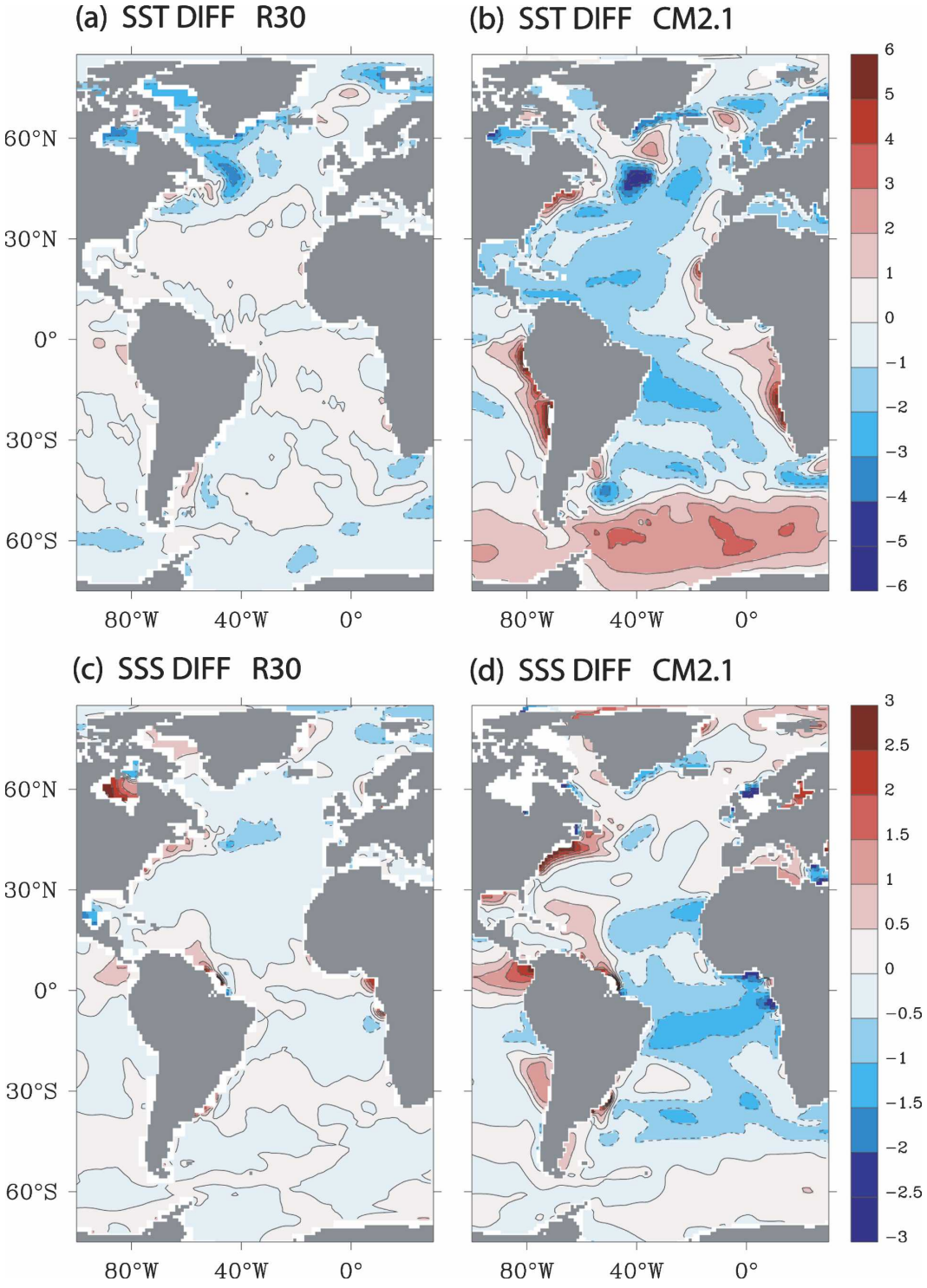

FIG. 1. The bias of SST and SSS in R30 and CM2.1 in comparison with Levitus observations (2001; provided by the National Oceanographic Data Center; http://www.nodc.noaa.gov). The data show simulation minus observation. Units: temperature (°C) and salinity (psu).

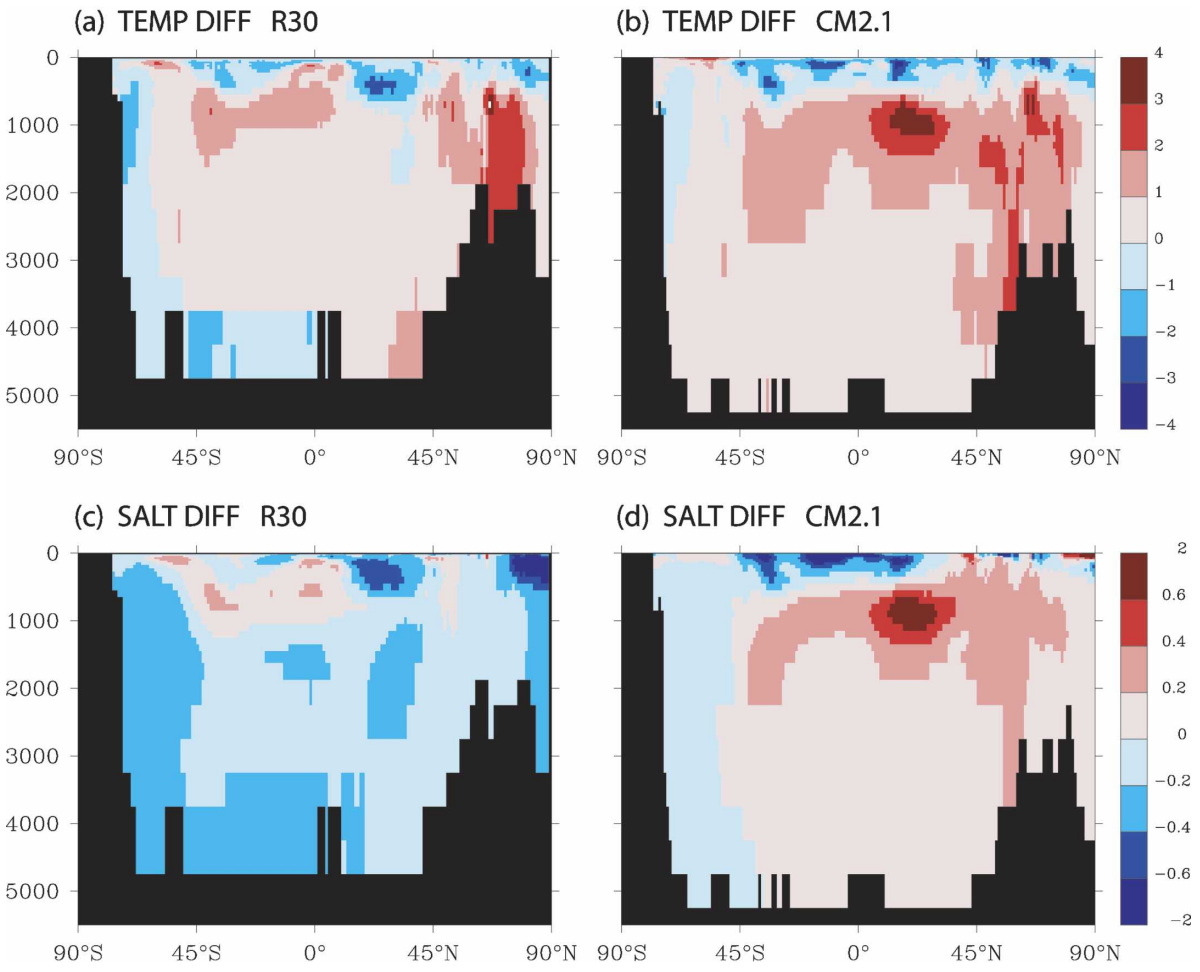

FIG. 2. As in Fig. 1 but for zonally averaged temperature and salinity in the Atlantic.

THC in many climate models (Stouffer et al. 2006a). The total amount of freshwater input during the 100-yr hosing period is about 3.2×10^{15} m^3, which would add about 9 m of globally averaged sea level. This freshwater perturbation is much stronger than many melting water releases in the past. For example, the total water drainage from Laurentide lakes during the cold event of 8200 yr ago is about 2×10^{14} m^3 (Barber et al. 1999; Clarke et al. 2003). A sea level rise of about 9 m has also been caused by the massive iceberg discharges into the North Atlantic during the Heinrich events (Chappell 2002). These discharges could induce a freshwater flux on the order of 0.1 Sv over a millennial time scale. It is worth noting that a freshwater anomaly of 1.0 Sv is very unlikely to happen again in the future unless the entire Greenland ice sheet melts completely within one century (Huybrechts and de Wolde 1999; Rignot and Kanagaratnam 2006)—a very unlikely occurrence. A broad perturbation region is chosen to ensure that both models can handle the large perturbation. The reason is that the input of a large freshwater flux into a small and localized ocean region can cause numerical problems, particularly in R30 which employs the virtual salt flux parameterization (Griffies et al. 2006). The freshwater perturbation is switched off at the end of the 100th year. The model integrations continue for another 200-yr period to study whether or not the THC recovers. In addition to the standard 1.0-Sv experiment, a 2.0-Sv hosing run with CM2.1 has also been carried out to ensure that the reversibility of the THC is not due to a different magnitude of the external freshwater threshold in CM2.1. The 2.0-Sv hosing run is similar to the 1.0-Sv case except that the magnitude of the freshwater perturbation is doubled.

3. Comparison of the water-hosing experiment

a. Behavior of the THC

Both R30 and CM2.1 simulate a similarly vigorous THC with pronounced multidecadal variations (Figs. 3

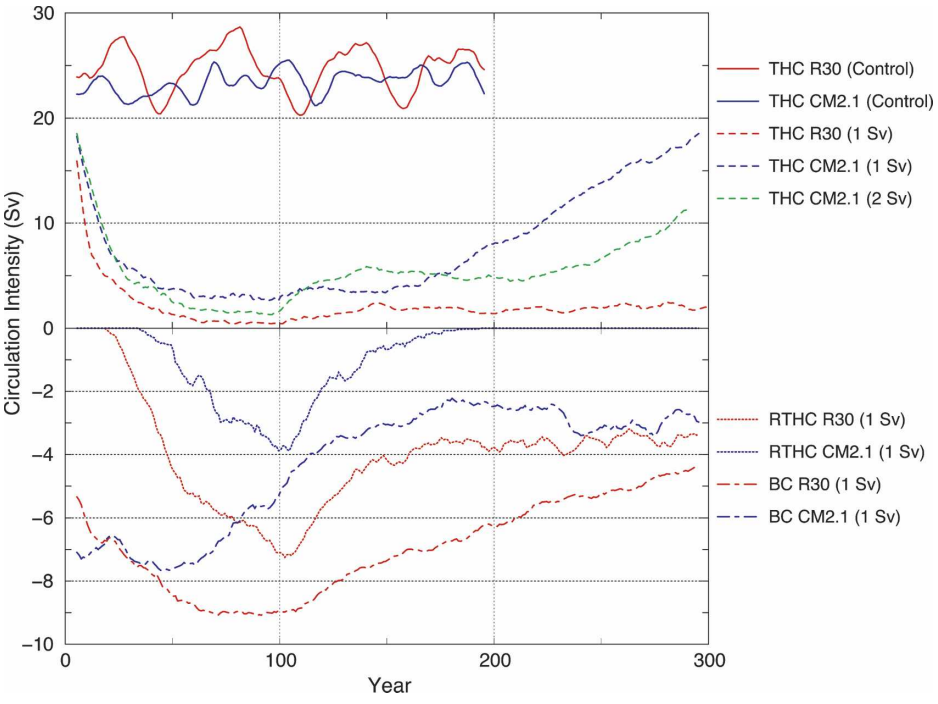

FIG. 3. Time series of the intensity of the THC, RTHC, and the bottom circulation (BC). The THC intensity is defined as the maximum meridional streamfunction value in 30°S–90°N, 500–3000 m. The RTHC intensity is the minimum streamfunction value at 30°S and between 200 and 1000 m. The BC intensity is the minimum streamfunction value below 2500 m. In the hosing experiments, the freshwater perturbation is removed at the end of the 100th year.

and 4. The long-term mean THC intensity in CM2.1 is about 23 Sv, while it is slightly stronger in R30 (24 Sv). The intensity of the THC is defined here as the maximum positive value of the MOC streamfunction in the North Atlantic Ocean, excluding the upper 500 m to eliminate the wind-driven cells. In addition, the multidecadal variations of the THC in R30 tend to have longer period and larger amplitude than those in CM2.1 (Fig. 3). The THC oscillations seen in the R30 control over this interval are larger and more regular than those found in the rest of a long-term integration (Delworth et al. 2002). In general, the THC seems reasonably well simulated in the control runs of both models.

In response to the 1.0 Sv freshwater input, the THC shuts down rapidly in both models with a slightly greater rate of decrease in R30 (Fig. 3). However, the curves tend to approach different stabilization levels with time. After 50 yr the THC intensity is very close to zero in R30 but is still about 3 Sv in CM2.1. These results indicate different freshwater sensitivity of the THC in these two models. The THC in CM2.1 is resistant to a complete shutdown even under the continuing 1.0-Sv freshwater forcing. After the removal of the freshwater perturbation, the THC remains inactive in R30 during the following 200-yr integration but recovers rapidly in CM2.1 after several decades. The THC in the 2.0-Sv hosing experiment with CM2.1 also recovers after the perturbation is terminated, although the recovery is much slower than that in the 1.0-Sv case (Fig. 3).

It is widely believed that the irreversible shutdown of the THC is caused by the internal dynamics, that is, the strong positive feedbacks involved in the THC such as that between the THC intensity and northward salt transport (Stommel 1961; Cubasch et al. 2001). There is potentially a critical strength of the THC, below which the behavior of the circulation is no longer controlled by the time scale of the forcing, but rather determined by its internal dynamics. According to Fig. 3, the strength of the THC stabilizes at a level very close to zero in both R30 and CM2.1. At this state, it is likely that the THC cannot be sustained by itself and should be attracted into the off regime if the off state is stable. The recovery of the THC in both the 1.0- and 2.0-Sv cases indicates that the off state of the THC in the water-hosing experiments is unstable in CM2.1. Therefore, the stability property of the THC is very different in R30 and CM2.1.

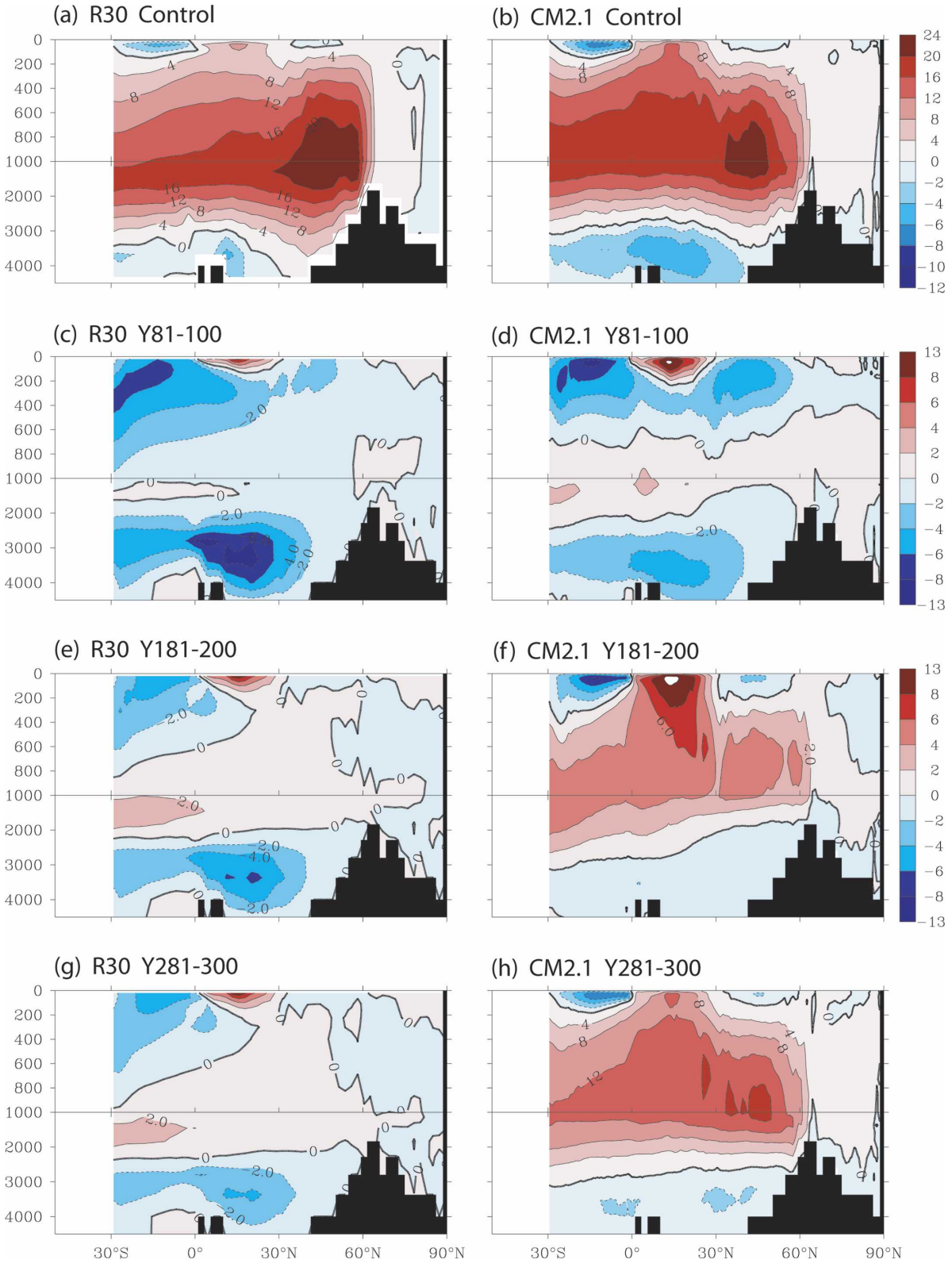

FIG. 4. The MOC patterns in the control run and the 1.0-Sv water-hosing experiment. (left) R30 and (right) CM2.1. (a), (b) The control run (200-yr mean); (c), (d) Y81–100 of the hosing experiment; (e), (f) Y181–200 of the hosing experiment; and (g), (h) Y281–300 of the hosing experiment. Panel (g) uses the same scale as (e) and (f); (h) uses the same scale as (a) and (b).

The meridional overturning streamfunction averaged over the last two decades of the hosing period, Y81–100 (Y ≡ year) shows distinctly different patterns between these two models (Figs. 4c and 4d). In R30 there is virtually no clockwise circulation (Fig. 4c) below 200 m in the entire Atlantic. The most notable feature, a reversed (counterclockwise in Fig. 4c) thermohaline circulation (RTHC), appears in the upper 1000 m of the South Atlantic. In CM2.1, however, there is a region between 600 and 2000 m, particularly in the South Atlantic where the circulation is still clockwise. It is likely that this weak THC is responsible for the THC recovery in CM2.1 (Fig. 3).

b. The role of the RTHC in R30

The shutdown of the THC leads to a very sluggish deep Atlantic in R30. The still active dynamical process in the upper 1000 m is thus critical to determining the behavior of the THC after the hosing is removed. According to Fig. 4c, the most notable feature in R30 is the RTHC in the upper 1000 m of the South Atlantic, which becomes well developed by the end of the hosing period. The formation of the RTHC in R30 is a result of the reversal of the North Brazil Current in the upper 400 m (Fig. 5). The THC consists of a series of narrow western boundary currents in the control run (Figs. 5a and 5d). After the shutdown of the THC, all western boundary currents weaken and the most significant change in the upper 400 m occurs along the east coast of South America (Fig. 5c). The North Brazil Current changes its direction from northwestward (Fig. 5a) to southeastward (Fig. 5b). Meanwhile, the Brazil Current accelerates. The reversed North Brazil Current connects to the Brazil Current, flowing all the way into the Southern Ocean along the continental shelf of the South America. There is notable seawater convergence at 40°–50°S near the east coast of the South America (Fig. 5b), corresponding to the sinking region of the RTHC. The currents in the 400–1000-m layer also become weaker (Figs. 5d–f), but the magnitude of the change is much smaller than that in the upper 400 m. Due to the mass convergence in the Caribbean Sea and surrounding regions (Fig. 5e), upwelling takes place there. Meanwhile, the southward return flow of the subtropical gyre in the eastern North Atlantic becomes stronger and more pronounced (Fig. 5b). This results from the increase of the wind stress and the southward propagation of the freshwater cap (Fig. 12a), which prevents the energy dissipation of the surface ocean flow through the vertical mixing process.

The RTHC is associated with the reversed meridional density gradient in the Atlantic (Fig. 14) and closely related to the circulation of Antarctic Intermediate Water (AAIW), which forms near the southern tip of South America in the present climate (Saenko et al. 2003). AAIW is characterized by water temperatures of 2°–4°C and salinity of about 34.2 psu, significantly fresher than Western Atlantic Sub-Arctic Water and Labrador Sea Water (Talley 1996). The intensity of the RTHC in R30 can be as large as 8 Sv at the end of the hosing period (Fig. 3). The RTHC weakens once the hosing is terminated (Figs. 3, 4e, and 4g) but remains active for the following 200-yr period, implying that it is a stable and self-sustaining circulation in R30. The upwelling of AAIW in the subtropical North Atlantic associated with the active RTHC is very pronounced and efficiently replaces the high salinity thermocline water there with the low salinity water from the Southern Ocean. This replacement prevents the rapid salinity recovery in the subtropical North Atlantic, which would be otherwise induced by the excess evaporation there after the termination of the hosing. The freshwater transport associated with the RTHC and the freshwater budget for the Atlantic Ocean will be analyzed in detail in the following section.

The freshwater input into 50°–70°N creates a sharp sea surface salinity (SSS) gradient at about 40°N latitude in both R30 and CM2.1 (Fig. 6a). After the termination of the hosing, this gradient at 40°N becomes much weaker in R30 due to the slow recovery of salinity in the subtropical North Atlantic and the rapid recovery of salinity in the perturbation region resulting from the downward mixing of the freshwater cap (Figs. 6b–f). The slow recovery of salinity at the subtropical North Atlantic is primarily a result of the freshwater transport and convergence associated with the RTHC. Given that the subtropical North Atlantic is a critical region to regulate the THC, the THC cannot restart because of the low salinity at the tropical–subtropical Atlantic. Figure 7 is a schematic cartoon to show how different systems in the Atlantic work together to stabilize the off state of the THC in R30. In contrast, the salinity increase at the subtropical North Atlantic is more rapid in CM2.1 and the SSS gradient at 40°N remains strong even without the external freshwater forcing (Figs. 6b and 6c). It is this rapid and complete salinity recovery in the subtropical North Atlantic that leads to the recovery of the THC in CM2.1 (section 3d).

c. Freshwater transport and budget analysis for R30

The freshwater transport and budget analysis in the Atlantic Ocean is presented to better understand the role of the RTHC and other processes in the behavior of the THC. The shutdown of the THC and formation of the RTHC greatly change the meridional salt/

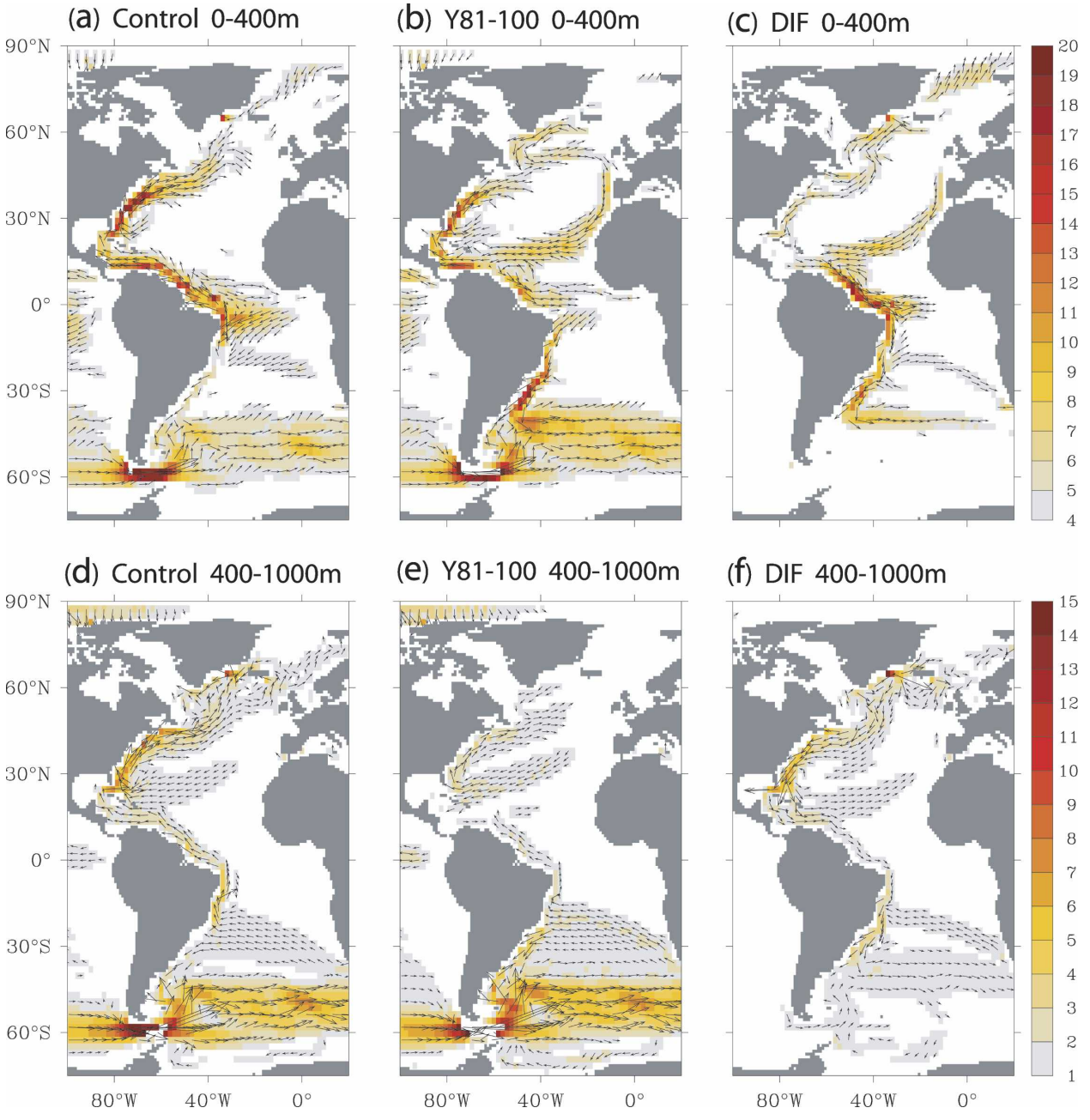

FIG. 5. The ocean currents in the control run and hosing experiment of R30. (a), (b), (c) The mean ocean currents in the upper 400 m; (d), (e), (f) the mean ocean currents in 400–1000 m. (a) and (d) The control run; (b) and (e) the 1.0-Sv hosing experiment; and (c) and (f) the difference (hosing minus control). Arrow shows the current direction and the shading indicates the velocity of the currents (cm s^{-1}).

freshwater transport in R30. The meridional salt transport in the Atlantic Ocean (F) can be decomposed into three components: the net mass/volume transport (F_{NM}), the meridional overturning (F_{OT}), and the horizontal circulations (F_{HOR}; Bryden and Imawaki 2001). Thus

$$F = \int\int \rho s v \, dx \, dz = \rho \langle v \rangle^{xz} \langle s \rangle^{xz} \int L(y, z) \, dz + \rho \int \langle v \rangle^{x} \langle s \rangle^{x} L(y, z) \, dz + \rho \int\int v' s' \, dx \, dz = F_{\mathrm{NM}} + F_{\mathrm{OT}} + F_{\mathrm{HOR}}, \quad (1)$$

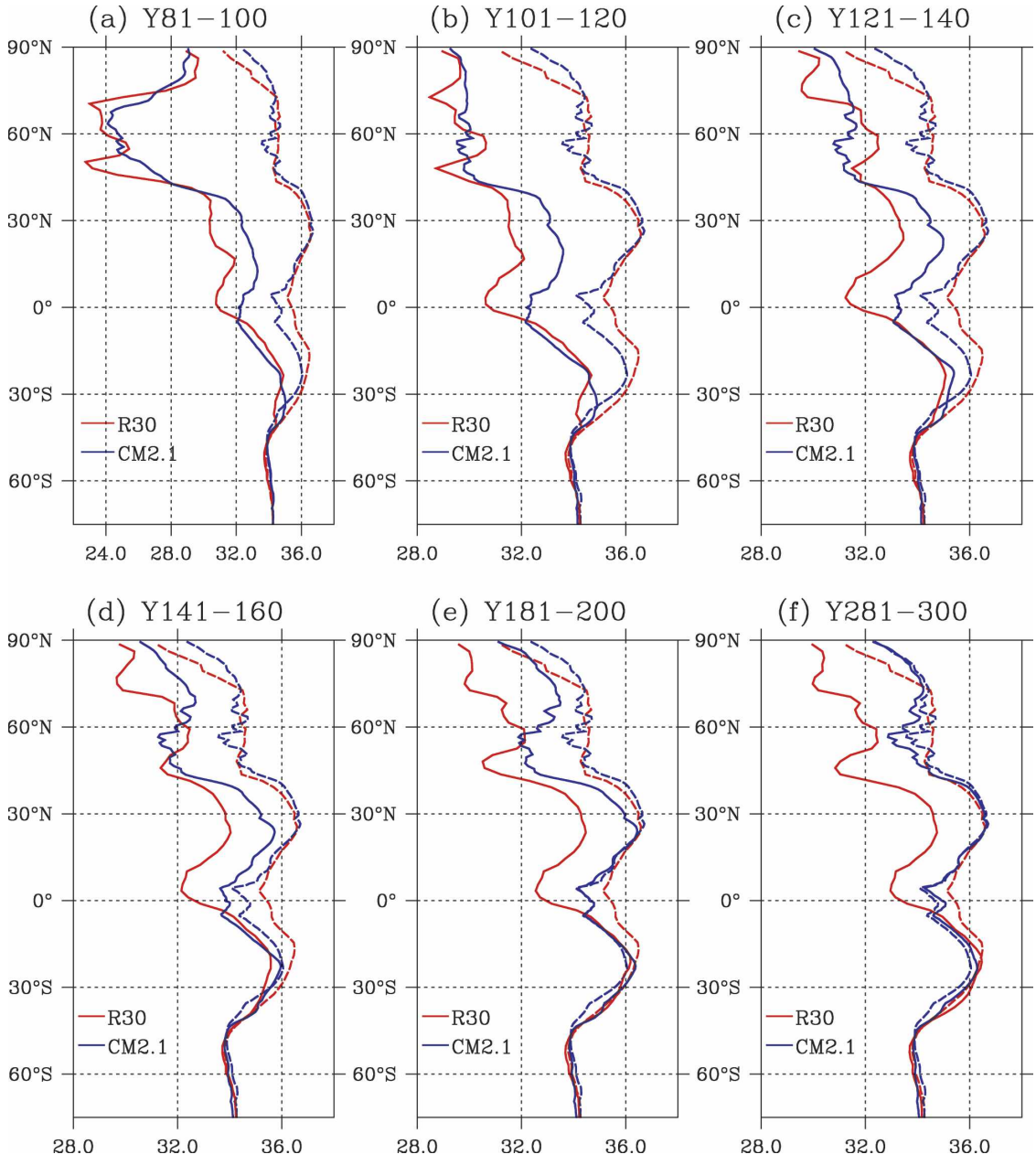

FIG. 6. The SSS zonally averaged in the Atlantic Ocean from the water-hosing experiment. The solid curves show the hosing runs averaged over a 20-yr period; the dashed curves show the long-term mean of the control run. (a) The last 20 years of the hosing; (b)–(f) 20-yr periods after termination of the hosing.

where s and v denote salinity and meridional velocity in the Atlantic Ocean, ρ is the seawater density with its variations neglected here, $L(y, z)$ is the length of the Atlantic basin in the zonal direction at each level, and $\langle\rangle^x$ and $\langle\rangle^{xz}$ denote the zonal and basin vertical cross-sectional average.

$$\langle v\rangle^x(y, z) = \langle v(x, y, z) - \langle v\rangle^{xz}(y)\rangle^x$$
$$v'(x, y, z) = v(x, y, z) - \langle v\rangle^{xz}(y) - \langle v\rangle^x(y, z). \quad (2)$$

Based on the salt transport, we estimate the freshwater transport by the overturning and horizontal circulations using a reference salinity (35 psu). To eliminate the physically unrelated part in F_{NM}, the transport of salinity anomaly with respect to the average salinity in the Atlantic (35 psu) is first calculated and then converted to a freshwater flux. Because the net oceanic volume exchange between different ocean basins is zero by construction in R30 and the virtual salt flux scheme is em-

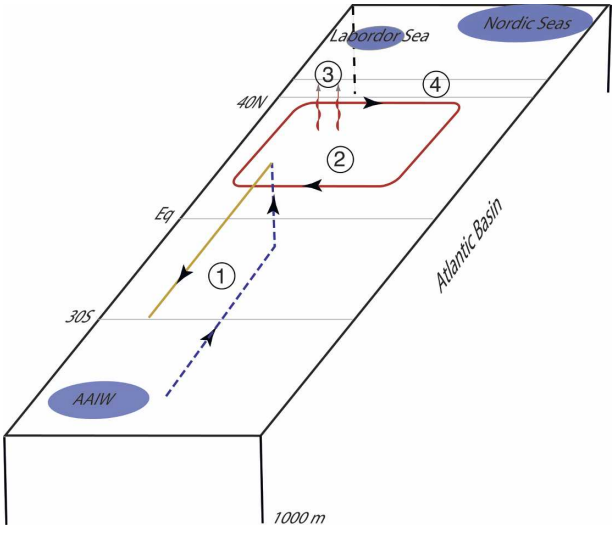

FIG. 7. Schematic illustration of how different systems in the Atlantic work together to stabilize the off state of the THC in R30. Process 1: the RTHC transports the fresh AAIW to the subtropical North Atlantic; process 2: the gyre circulation distributes the low salinity water in the subtropical region; process 3: the excess evaporation tends to enhance the salinity over the subtropical region; process 4: the northward mixing of salt across the frontal zone at about 40°N is much weaker in R30 (compared with that in CM2.1). The off THC state gets to equilibrium when freshwater gain (process 1) balances freshwater loss (process 3).

ployed at the ocean surface, there is no net mass/volume transport component for R30 ($F_{NM} = 0$).

The evolution of the components of the meridional freshwater transport is shown in Fig. 8. In the control run of R30, the freshwater transport associated with the overturning circulation is almost uniformly southward (Fig. 8a, black curve). The maximum southward transport occurs near 30°N with magnitude up to 0.5 Sv, comparable to previous estimates (Rahmstorf 1996). At the end of the hosing period (Y81–100), the maximum freshwater transport by the overturning shifts to 40°–50°N, while the horizontal component changes its direction from northward to southward in the 0°–50°N latitude band (Figs. 8a and 8b, blue curves). In R30, the overturning and horizontal circulations work together to transport the perturbation freshwater southward. After termination of the hosing, the freshwater transport quickly stabilizes toward a pattern very different from the control (Figs. 8a and 8b, green and red curves). The freshwater transport by the overturning becomes mainly northward south of 40°N as a result of the formation of the RTHC. The maximum northward freshwater transport by the overturning occurs at about 10°N with magnitude up to 0.25 Sv.

Table 2 shows the freshwater budget analysis for the Atlantic Ocean. During the "on" state of the THC (the control of R30), the freshwater import into the Atlantic basin by the horizontal circulation dominates the freshwater export by the overturning at 30°S. The formation of the RTHC in the hosing experiment leads to a reversal of the freshwater transport at 30°S and ~0.2 Sv increase in the freshwater import into the Atlantic by the overturning (Y281–300). During the off state of the THC, the overturning component (0.132 Sv) becomes the dominant term in the oceanic freshwater transport, much larger than the horizontal component (0.030 Sv). The change in the total oceanic freshwater transport at 30°S induced by the shutdown of the THC is comparable to a previous estimate using an EMIC (Gregory et al. 2003). At 60°N the horizontal circulation imports freshwater into the Atlantic basin from the Arctic in the control climate. This freshwater import gets much weaker after the shutdown of the THC. Consequently, during the off state of the THC, the freshwater transport by the RTHC at the southern end of the Atlantic Ocean contains most of the oceanic freshwater transport that influences the mean salinity of the Atlantic Ocean.

In terms of the oceanic freshwater convergence (Table 3), a strong freshwater convergence (0.220 Sv) is induced by the active THC to compensate the excess evaporation (−0.534 Sv) in the subtropical North Atlantic in the control climate of R30. A stable climate state without an active THC therefore requires an alternative mechanism to converge freshwater into the subtropical North Atlantic and stabilize the salinity. Otherwise, the salinity would keep increasing, and eventually lead to a recovery of the THC. According to Table 3, a 0.257-Sv freshwater convergence is induced by the overturning (Y281–300). Therefore in the off state of the THC, the RTHC plays a similar role to the THC in the on state by compensating the freshwater loss in the subtropical North Atlantic. Although the horizontal circulation is important in distributing the freshwater within the gyre (Fig. 8), its role in influencing the salinity of the subtropical North Atlantic is secondary compared with that of the overturning circulation (Table 3).

The atmosphere provides complex feedbacks to the shutdown of the THC. The atmospheric feedbacks include an overall increase in the net evaporation over the Atlantic Ocean and a southward shift of the Atlantic ITCZ (Fig. 9), both of which are negative feedbacks to the THC shutdown. According to Table 2, by Y281–300 the Atlantic Ocean with an inactive THC in R30 is slightly more evaporative by 0.035 Sv than in the control climate. In addition, due to the southward shift of the Atlantic ITCZ, the subtropical North Atlantic is more evaporative by 0.073 Sv (Table 3). The role of the

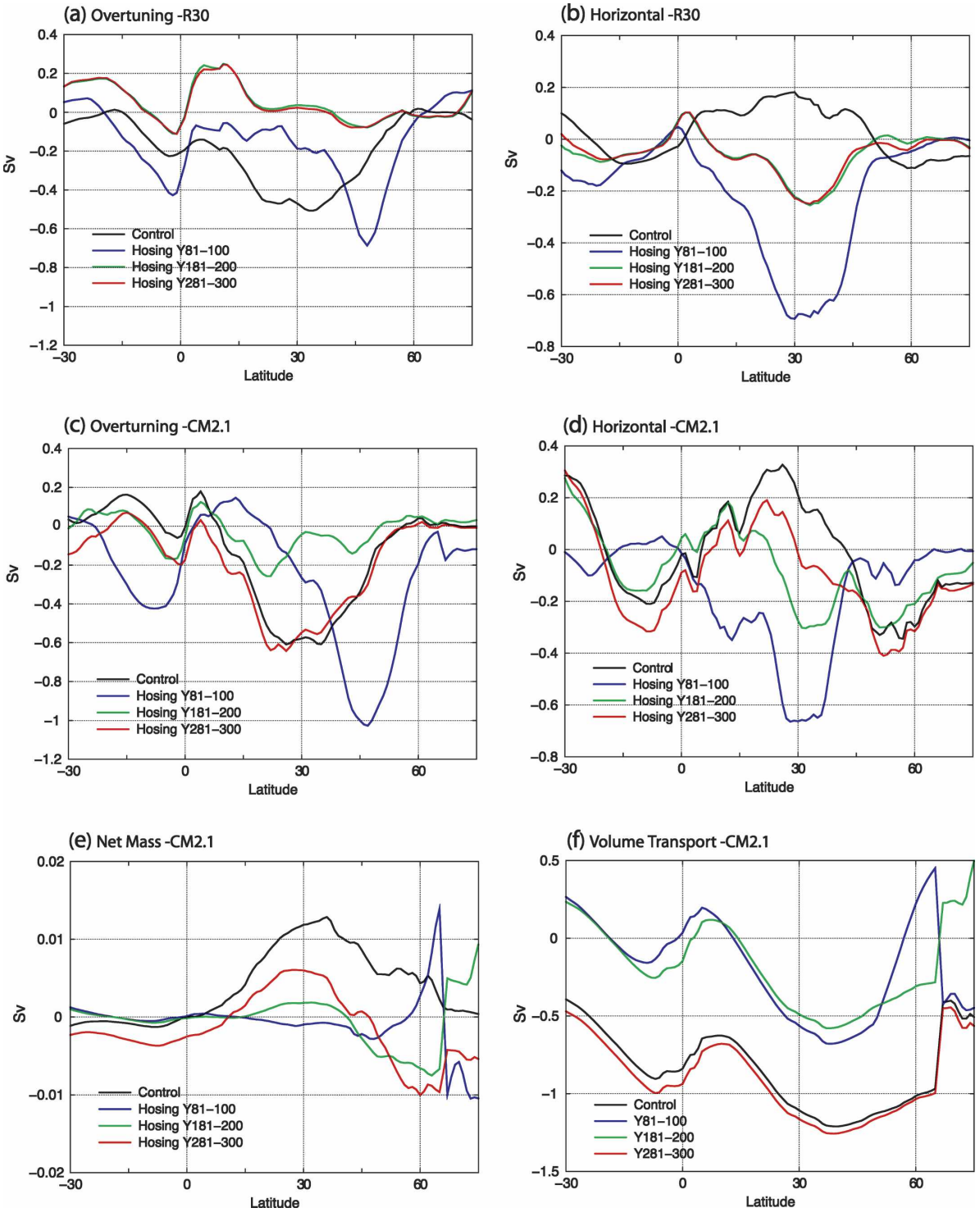

FIG. 8. Freshwater transport in the Atlantic Ocean: (a), (c) The overturning component; (b), (d) the horizontal component; (e) the net mass flux component in CM2.1; (f) the net volume transport in CM2.1.

atmospheric feedbacks in the freshwater budget of the subtropical North Atlantic is secondary compared with that of the RTHC in R30. But the atmospheric feedback is much stronger in CM2.1 and plays a more important role in impacting the behavior of the THC (section 3d). Many other climate models also simulated a pronounced southward shift of the Atlantic ITCZ after the shutdown of the THC (Vellinga et al. 2002; Loh-

TABLE 2. The analysis of the freshwater budget for the Atlantic Ocean (30°S–60°N) in the control run and hosing experiment (unit: Sv). Downward fluxes at the ocean surface indicated by positive values. The dominant term of the three components of the oceanic freshwater transport is indicated by boldface. See Eq. (1) for details.

	Northward transport at 30°S			Northward transport at 60°N						
	Overturning	Horizontal	Net mass	Overturning	Horizontal	Net mass	$P - E + R$	Flux adjustment	Perturbation	Total
					R30					
Control	−0.060	**0.118**	0	0.012	**−0.136**	0	−0.615	0.345	0	−0.088
Y81–100	0.052	**−0.114**	0	**−0.055**	−0.044	0	−0.520	0.345	0.616	0.280
Y181–200	**0.133**	−0.009	0	**−0.018**	−0.013	0	−0.626	0.345	0	−0.126
Y281–300	**0.132**	0.030	0	−0.015	**−0.034**	0	−0.650	0.345	0	−0.094
					CM2.1					
Control	0.034	**0.285**	0.001	0.039	**−0.298**	0.004	−0.609	0	0	−0.034
Y81–100	**0.049**	−0.010	0.001	**−0.117**	−0.006	−0.006	−0.495	0	0.616	0.290
Y181–200	−0.012	**0.275**	0.001	0.023	**−0.211**	−0.007	−0.570	0	0	−0.111
Y281–300	−0.146	**0.304**	−0.002	−0.003	**−0.316**	−0.010	−0.604	0	0	−0.121

Total = (northward transport at 30°S) − (northward transport at 60°N) + $(P - E + R)$ + (flux adjustment) + (perturbation).

mann 2003), although the exact magnitude of the precipitation anomaly varies among models. It should be noted that the flux adjustment employed in R30 is a large term in the water budget, offsetting about half of the net freshwater loss of the Atlantic Ocean (Tables 2 and 3). The possible role of the flux adjustments is discussed further in section 5.

d. The recovery process of the THC in CM2.1

At the end of the hosing period, the North Brazil Current becomes reversed in CM2.1 (Figs. 10a–c), similar to what occurred in R30. Unlike the case in R30, however, the North Brazil Current does not connect to the Brazil Current. The convergence of the seawater in the upper 400 m and the major downwelling associated with the RTHC take place at about 20°S near the east coast of Brazil (Fig. 10b). The RTHC in CM2.1 is linked closely to the surface Ekman cell (Fig. 4c). So the RTHC in CM2.1 mostly involves the water in the low-latitude upper thermocline, where salinity and temperature do not vary much spatially. The intrusion of AAIW from the Southern Ocean and its upwelling in the subtropical North Atlantic is weak. After the termination of the hosing, the RTHC weakens rapidly and eventually disappears (Fig. 3). Only the wind-driven Ekman cell remains in the upper 200 m (Fig. 4h).

In the control climate of CM2.1, the freshwater transport by the horizontal circulations at 30°S (0.285 Sv) and 60°N (−0.298 Sv) almost completely compensate the net surface water flux $(P - E + R)$ over the Atlantic Ocean (−0.609 Sv: Table 2). Of course, any decomposition of the ocean circulations is arbitrary. A complete separation of different types of circulations is impossible because of their integration in the ocean. So the horizontal circulation component here, represented by the $v's'$ term in Eq. (1), may include some contribution from the overturning circulation under some circumstances. The freshwater transports by the overturning circulation and net mass flux are relatively small (Figs. 8c–e). During the hosing experiment, the hori-

TABLE 3. The freshwater convergence in the subtropical North Atlantic (10°–40°N) induced by different processes (unit: Sv). The dominant term of the three components of the oceanic transport is indicated by boldface.

	Overturning	Horizontal	Net mass	$P - E + R$	Flux adjustment	Total
			R30			
Control	**0.220**	0.038	0	−0.534	0.214	−0.062
Y81–100	0.192	**0.460**	0	−0.609	0.214	0.257
Y181–200	**0.242**	0.146	0	−0.605	0.214	−0.003
Y281–300	**0.257**	0.128	0	−0.607	0.214	−0.008
			CM2.1			
Control	**0.448**	0.113	−0.008	−0.557	0	−0.004
Y81–100	**0.829**	0.006	0.001	−0.676	0	0.160
Y181–200	0.078	**0.312**	−0.001	−0.670	0	−0.281
Y281–300	**0.269**	0.211	−0.002	−0.574	0	−0.096

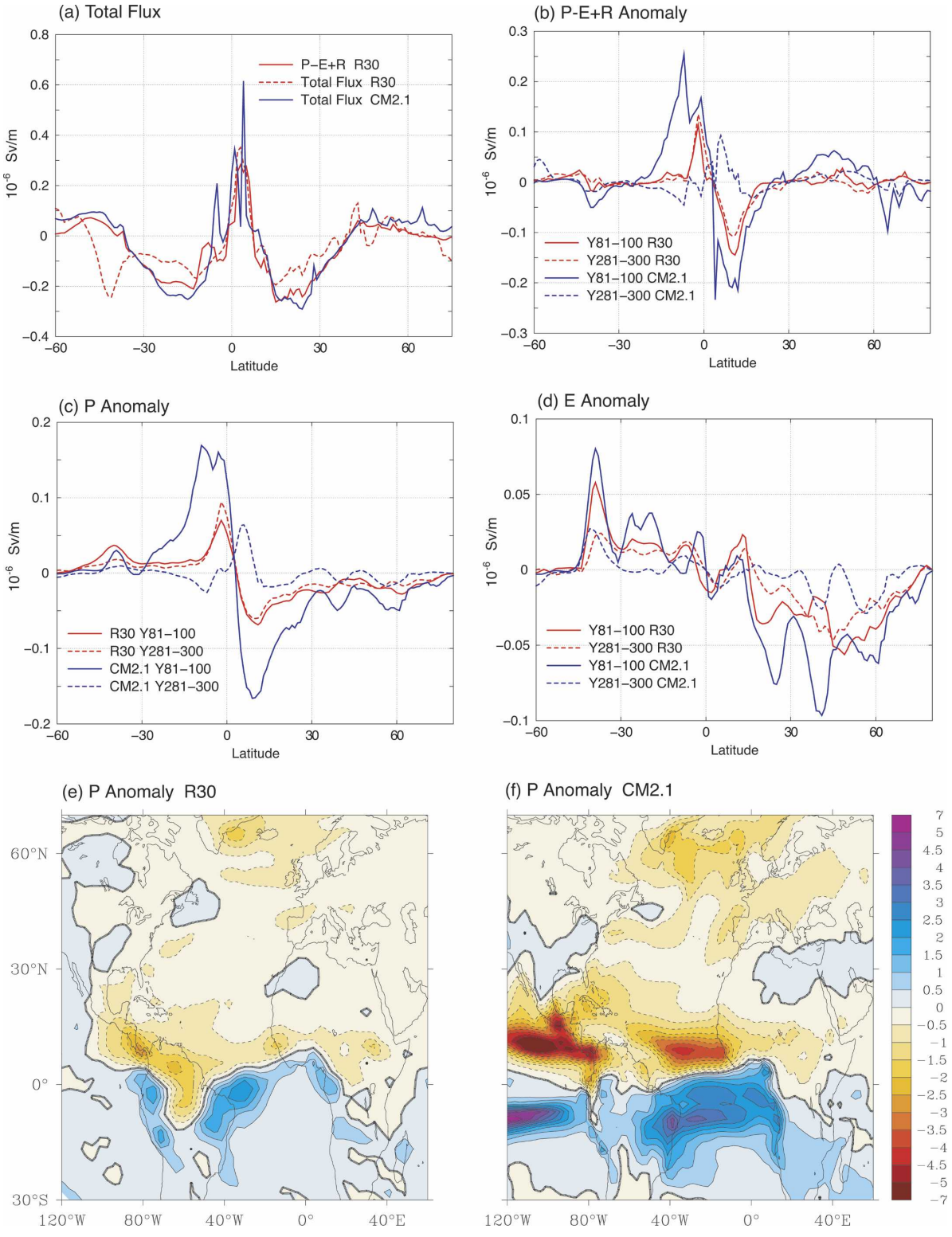

FIG. 9. (a)–(d) The net freshwater flux zonally integrated across the Atlantic and (e)–(f) the southward shift of the Atlantic ITCZ: (a) total flux in the control run; (b)–(d) the anomaly in the hosing experiment; (e), (f) Y81–100, unit: mm day^{-1}.

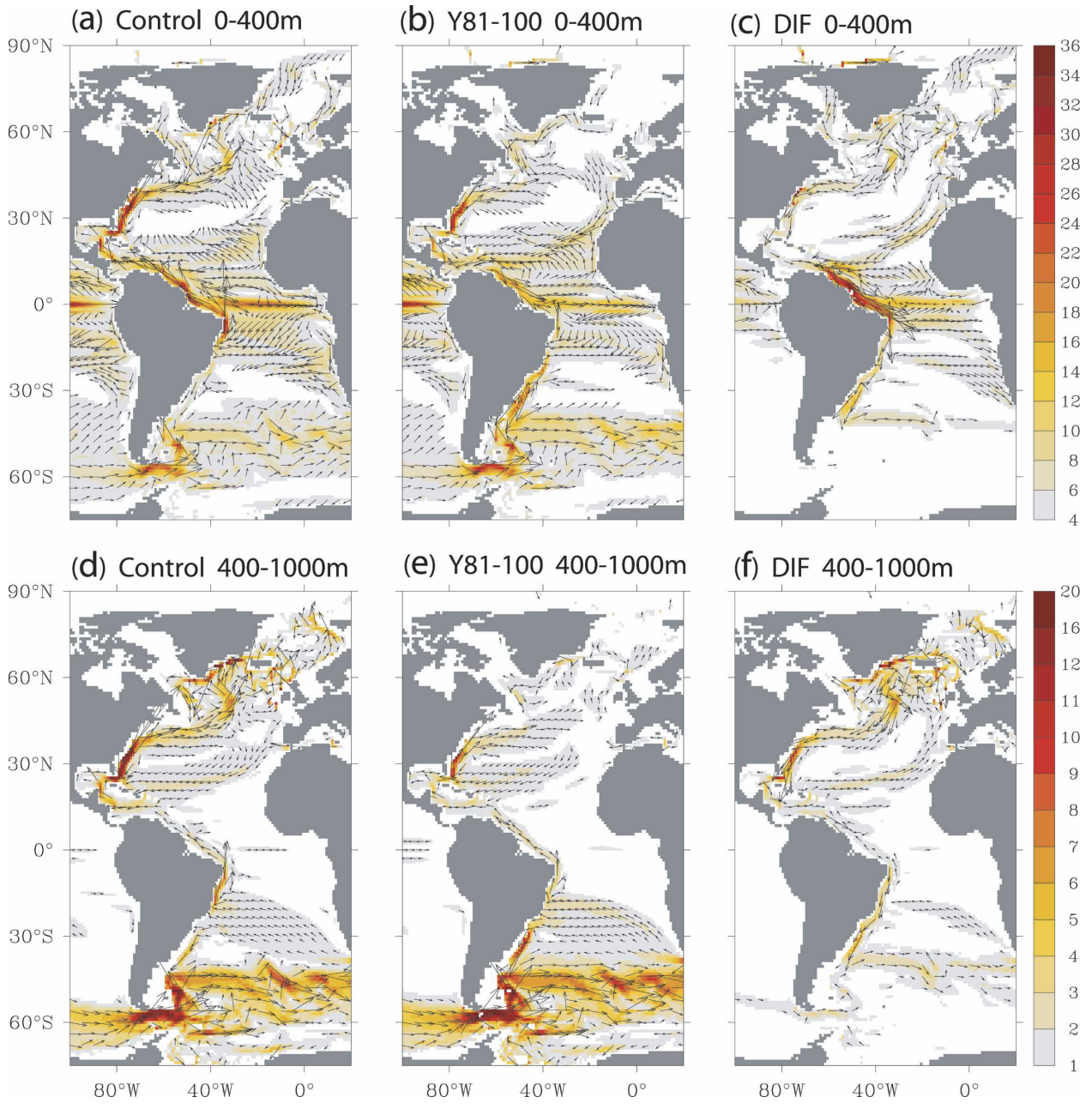

FIG. 10. The ocean currents in the control run and hosing experiment of CM2.1: (a)–(c) the mean ocean currents in the upper 400 m; (d)–(f) the mean ocean current in 400–1000 m for (a) and (d) the control run, (b) and (e) show the 1.0-Sv hosing experiment, and (c) and (f) the difference (hosing minus control). Arrow shows the current direction and the shading indicates the velocity of the currents (cm s^{-1}).

zontal circulation is the dominant term to balance the net freshwater loss to the atmosphere. The overturning component at 30°S changes from a slight freshwater import in the control to a freshwater export at Y281–300 of the hosing experiment, in contrast to the simulation of R30 (Table 2). For the subtropical North Atlantic, the freshwater convergence induced by the overturning, horizontal circulation and net mass flux cannot totally offset the net surface water flux after the termination of the hosing (Table 3). The net freshwater loss (−0.281 Sv during Y181–200) leads to a continuous increase in the subtropical salinity. This eventually causes the collapse of the RTHC and the reintensification of the THC.

The atmospheric feedback is much stronger in CM2.1 than in R30. The shutdown of the THC causes a sig-

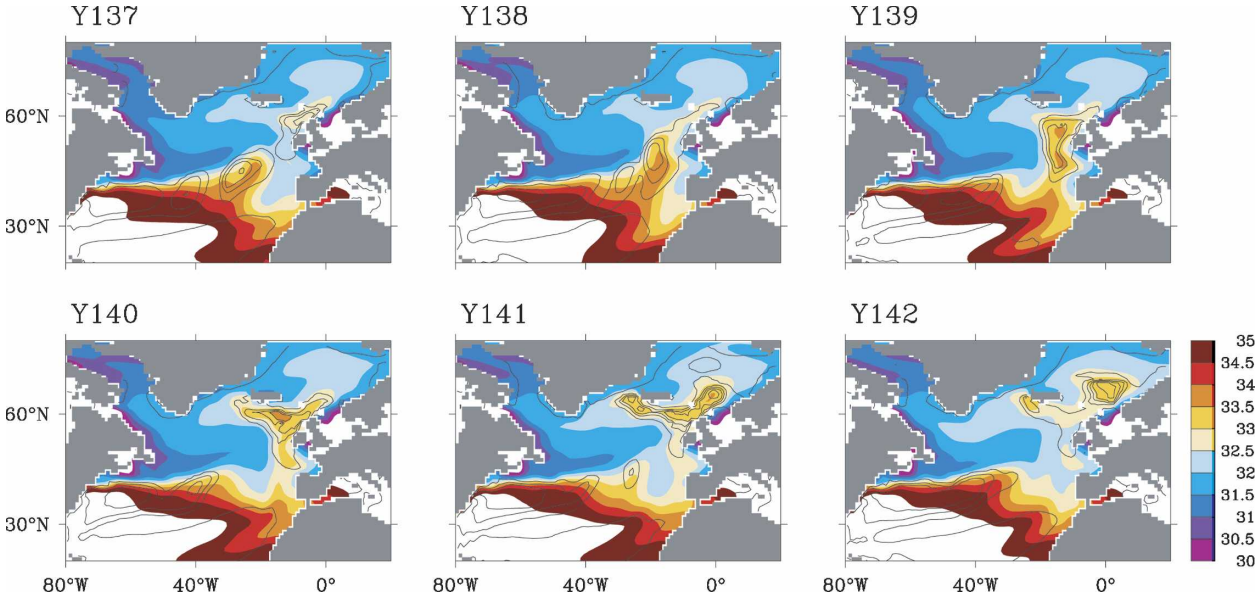

FIG. 11. The generation of a baroclinic eddy along the frontal region at about 40°N during the Y137–142 period in CM2.1. The eddy, after detached from the gyre circulation, propagates northward into the Nordic seas and Irminger Sea to restart the deep convection there. SSS (psu) is indicated by the shading and the contour lines show the mixed layer depth (m) with 100-m interval. The eddy is not yet detached at Y137 and Y138. It separates from the gyre at Y139 and propagates northward during Y140–143.

nificant southward shift of the Atlantic ITCZ in CM2.1 (Fig. 9). In addition to the magnitude of the response, the maximum drying in CM2.1 occurs over the ocean while it is over the land in R30 (Figs. 9e and 9f). The southward shift of the ITCZ in CM2.1 causes an anomalous freshwater loss of about 0.3 Sv in 0°–30°N of the North Atlantic. By contrast, this freshwater anomaly is much smaller in R30, with magnitude only about 0.1 Sv. The southward shift of the Atlantic ITCZ enhances the salinity in the subtropical North Atlantic and prevents the southward propagation of the perturbation freshwater. This enhancement of the salinity tends to inhibit the formation of the RTHC by increasing the upper-ocean density in its upwelling region.

In CM2.1, the salinity over the subtropical North Atlantic increases rapidly after the termination of the hosing, keeping the strong salinity gradient at about 40°N latitude. Without the external freshwater forcing, the ocean is free to evolve. The strong lateral density gradient and north–south current shear at 40°N can easily trigger baroclinic instability. Large-scale baroclinic waves and eddies are continuously generated along the 40°N frontal region. Owing to the fine resolution of the ocean component (1° at this latitude), these large-scale waves and eddies are well resolved in CM2.1. It should be noted that the mesoscale eddies cannot be resolved as the first baroclinic Rossby radius is less than 20 km at midlatitudes. Figure 11 demonstrates the process of the generation of a large-scale eddy and its northward propagation. The eddy is gradually becoming detached from the wind-driven gyre circulation, similar to ring shedding along the Gulf Stream. This eddy, rotating in the anticyclonic direction, then propagates northward after its separation from the gyre circulation into the Nordic seas and Irminger Sea. Thus, the original deep convection and deep-water formation regions are the preferable directions for the eddy to propagate. The mixed layer in this eddy gradually deepens during its northward movement. When it reaches the Nordic seas and Irminger Sea, the eddy initiates the deep convection and deep-water formation there. The recovery process of the THC and the SSS in the high latitudes in CM2.1 is governed by the continuous generation and northward propagation of the large-scale eddies.

The eddy propagation is a very efficient way to mix the ocean. Its contribution to the northward salinity transport and role in the dynamics of the THC is likely to have been underestimated in the previous research (Alley et al. 2003; Longworth et al. 2005; Schlesinger et al. 2006). In the classical two-box ocean model of Stommel (1961), the flow between the two ocean boxes is a purely overturning flow, which is closely related to the density differential of the two ocean boxes. The poleward salt transport is induced only by this flow with the contribution from the horizontal wind-driven circulation and mixing process totally neglected. In this case,

the THC presents remarkable nonlinearity and possesses two stable equilibria. However, when the salt transport induced by the mixing processes associated with the gyre circulation and eddy propagation is taken into account, the bistability of the THC weakens significantly (Saltzman 2002). Both the sharper north–south density gradient at about 40°N and the ability to resolve the oceanic large-scale eddy could contribute to the stronger horizontal mixing of salinity in CM2.1 than in R30, therefore leading to a weaker stability of the off THC state in CM2.1.

4. Processes influencing the simulation of the RTHC

a. Southward propagation of the salinity and temperature anomalies

The analyses in the preceding section have shown that the RTHC is well developed and stable in R30 and plays an important role in stabilizing the off state of the THC. Given the importance of the RTHC, it is desirable to study the critical processes that influence the simulation of the RTHC and its stability. Similar to the THC, the RTHC is also driven by the thermohaline effect, that is, the meridional pressure (density) gradient (Saenko et al. 2003). Thus, different responses of the meridional density gradient are the key to explain the different response of the RTHC among models.

Figures 4c,e,g indicate that the major upwelling associated with the RTHC takes place at low latitudes, especially beneath the wind-driven Ekman cell in the North Atlantic. The density of the subsurface seawater beneath the Ekman cell must be undergoing significant decrease to allow the strong upwelling there. The 1.0-Sv freshwater input causes considerable freshening over the perturbation region in both models (Figs. 12a and 12b). The relatively greater magnitude of the SSS response in R30 might result from its use of the virtual salt flux parameterization. After a freshwater cap quickly forms in the perturbation region in both models, it gradually spreads southward with the gyre circulation toward the tropical–subtropical Atlantic. According to Figs. 12a and 12b, the propagation of perturbation freshwater is more efficient and faster in R30 than in CM2.1. As a result, the Atlantic between 10°S and 30°N is overall fresher in R30 than in CM2.1 at the end of the hosing period with magnitude up to 3 psu (Fig. 12c).

The very low potential density of the freshwater cap inhibits its vertical mixing with the seawater below. Away from the surface, the maximum salinity decrease in the perturbation region and the route of the southward propagation of the freshwater along the eastern North Atlantic is indistinguishable at 200-m depth and below in both models (Figs. 13a and 13b). Unlike that at the surface, the maximum freshening at the subsurface layer occurs at the subtropical region of the North Atlantic. The subtropical gyre is predominately a downwelling region. The large freshening results from the subduction of freshwater after the high-latitude freshwater cap is advected into the gyre to significantly freshen its near-surface layer. Thus, the southward spread of the freshwater cap is almost purely horizontal until it reaches the subtropical region. The subduction associated with the gyre circulation plays a vital role in mixing the surface freshwater downward, reducing the density of the entire subsurface layer at the low latitudes, and therefore facilitating the formation of the RTHC. Due to the faster southward propagation of the freshwater, the subduction of freshwater is more pronounced in R30 (Figs. 13a and 13c). The beltlike maximum freshening at 200 m in CM2.1 (Fig. 13b) is more relevant to the enhancement of the vertical mixing due to the large surface cooling (Fig. 12e).

In contrast to the SSS anomaly, the southward propagation of the SST anomaly is more efficient and faster in CM2.1 than in R30. In CM2.1 the icy seawater formed in the perturbation region has been transported by the gyre circulation all the way into the Caribbean Sea at the end of the hosing period, causing a large cooling there (Fig. 12e). This southward transport of the SST anomaly is weaker in R30, and the cooling in the Caribbean Sea and surrounding ocean regions is much smaller (Fig. 12d). The great reduction of the northward heat transport from the South Atlantic induced by the shutdown of the THC also facilitates the temperature decrease in the Caribbean Sea and surrounding regions. Consequently, the low-latitude Atlantic is much warmer and fresher in R30 than in CM2.1 at the end of the hosing period.

b. Different response of the potential density

The different simulations in the southward propagation of the salinity and temperature anomalies result in different responses of the low-latitude seawater potential density. In the control integrations of both models, the meridional density gradient is similar in the upper Atlantic (Figs. 14c and 14f). The densest water is found at about 70°N and in the Southern Ocean, corresponding to NADW and AABW. The seawater potential density decreases rapidly from 70°N toward 30°N, but the gradient becomes very smooth between 30°N and 30°S.

In response to the large freshwater input, the potential density of the entire upper ocean north of 30°N

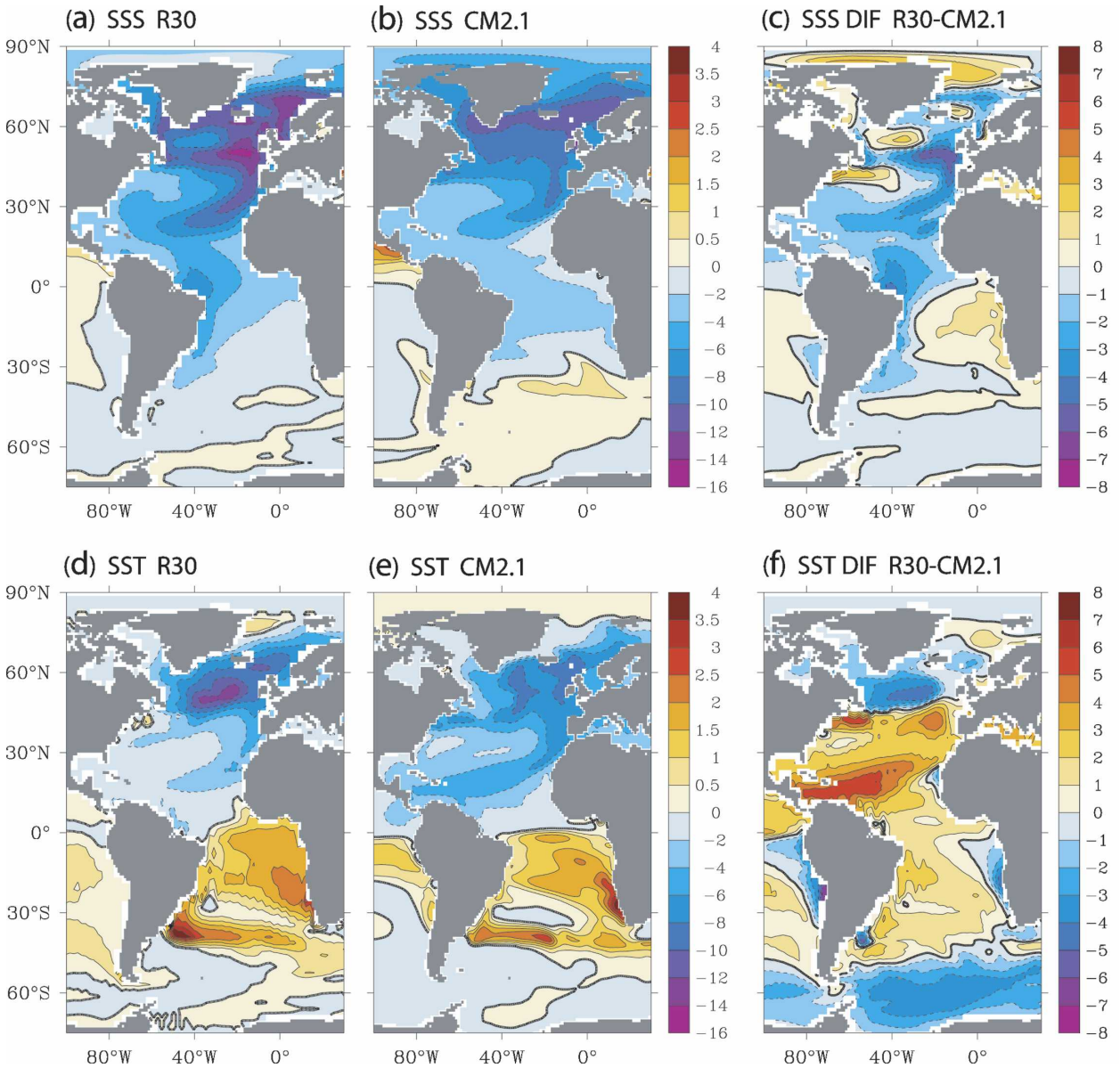

FIG. 12. The SSS (psu) and SST (°C) responses in the 1.0-Sv water-hosing experiment (Y81–100): the SSS anomaly (a) in R30 and (b) in CM2.1; (c) the SSS difference between R30 and CM2.1 (R30 minus CM2.1); the SST anomaly (d) in R30 and (e) in CM2.1 and (f) the SST difference between R30 and CM2.1.

decreases dramatically. This decrease in potential density becomes smaller toward the south with no apparent change in the Southern Ocean. Owing to the intensive downwelling of the freshwater at the subtropical North Atlantic in combination with the warm temperatures there, the seawater in the upper 400 m at about 30°N has the smallest surface potential density (<1024 kg m^{-3}), while the seawater in the Southern Ocean becomes the densest surface water mass (>1027 kg m^{-3}) at the end of the hosing period. As a result, the sharp gradient between 30° and 70°N in the control disappears, causing the shutdown of the THC. Instead, a sharp gradient forms between the Southern Ocean and 30°N with the gradient flipped into the opposite direction. This southward density gradient becomes steeper gradually with the southward propagation of the freshwater cap and the decrease of the potential density at low latitudes. Once beyond some critical point, the RTHC can develop in the upper Atlantic. Due to the faster propagation of the salinity but slower propagation of temperature, the decrease in the potential density at about 30°N is greater in R30 than in CM2.1 and

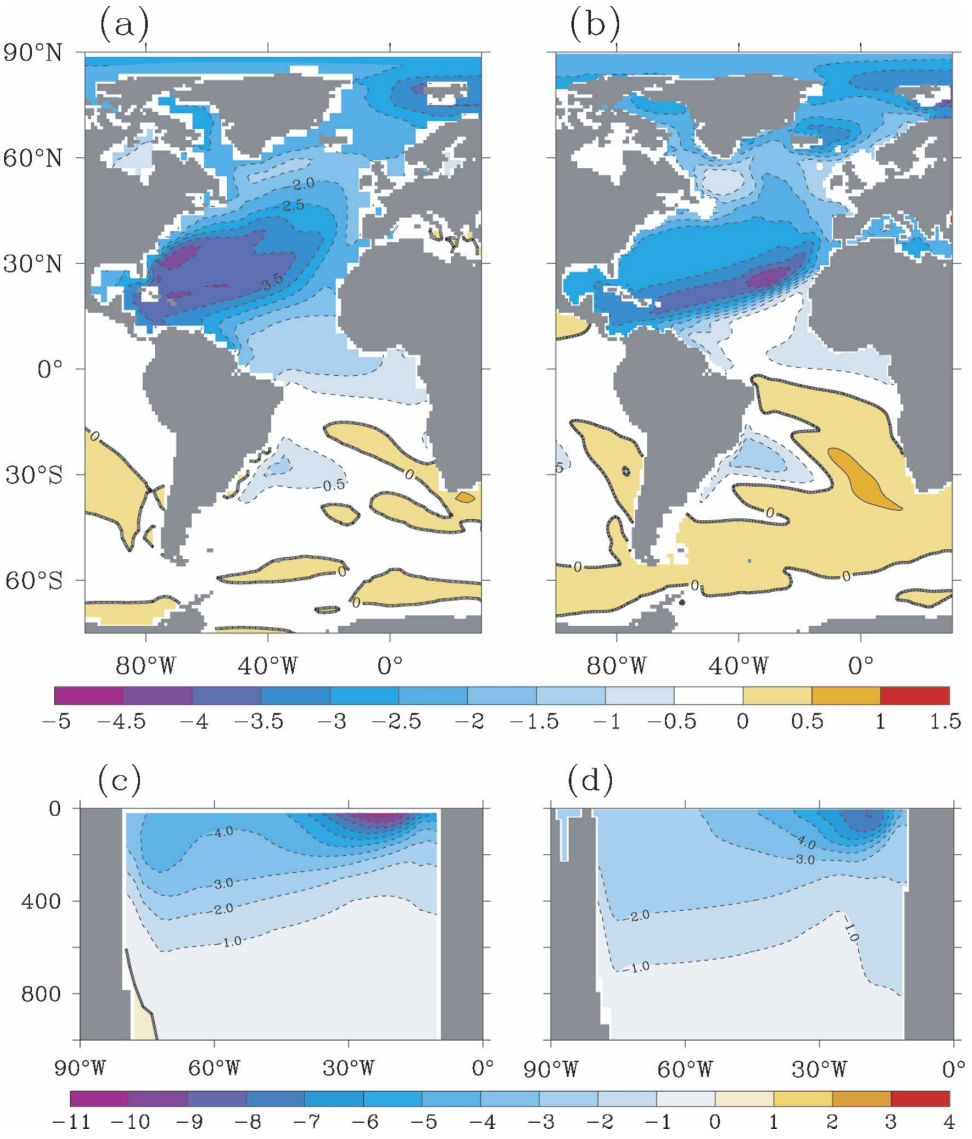

FIG. 13. Subduction of the perturbation freshwater in the subtropical North Atlantic (Y81–100): the salinity anomaly (a) at 200 m in R30 and (b) at 200 m in CM2.1; the vertical cross section (c) at 30°N in R30 and (d) at 30°N in CM2.1.

the southward density gradient is sharper, leading to a better developed RTHC.

5. Discussion and conclusions

It is well known that the THC is a self-sustaining system involving many complex feedback processes. Previous research suggested that the positive feedbacks are strong enough to make the THC bistable under the present climate forcing (Stommel 1961). There is strong positive correlation between the THC intensity and northward salt transport. A negative (positive) anomaly in the strength of the THC transports less (more) salt northward and tends to weaken (enhance) the THC further. If the weakening of the THC passes some critical point, an irreversible shutdown of the THC is possible. However, two AOGCMs developed and used at GFDL show differing results about the stability of the THC in the CMIP/PMIP coordinated water-hosing experiment. The "off" state induced by the external freshwater input is stable in R30, but unstable in CM2.1. This discrepancy is also found in other climate models. This paper analyzes in detail the simulations from R30 and CM2.1 and provides possible mechanisms responsible for the difference.

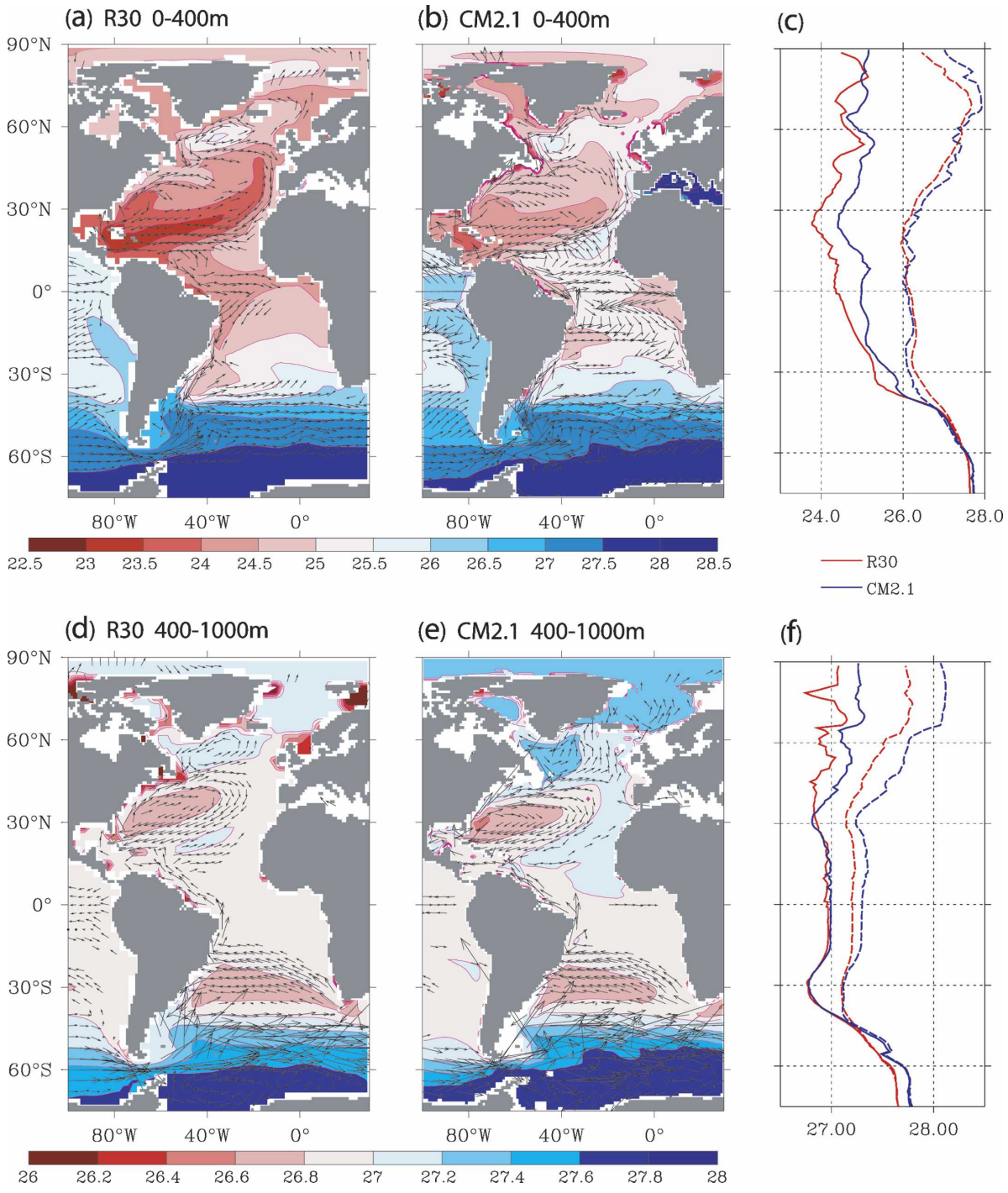

FIG. 14. Potential density σ (kg m^{-3}) and ocean current (cm s^{-1}) in the 1.0-Sv water-hosing experiment (Y81–100): the potential density (shaded) and ocean currents (a)–(c) in 0–400 m, (d)–(f) in 400–1000 m, and (c) and (f) the zonal mean of the potential density. Dashed lines denote controls; solid lines denote hosing experiments.

The difference in the THC stability properties is closely related to the simulation of the RTHC (reverse THC cell; Prange et al. 2003) in the South Atlantic Ocean and complex air–sea feedback. After the shutdown of the THC, the RTHC is vigorous and stable in R30—a model with a stable off state of the THC in the water-hosing experiment. It transports a large amount of freshwater (salt) into (out of) the Atlantic. Owing to

this freshwater transport from the Southern Ocean by the RTHC, the SSS in the subtropical North Atlantic recovers slowly after the termination of the hosing and eventually stabilizes at a level much lower than that in the control. The low salinity of the subtropical North Atlantic prevents the recovery of the THC. The RTHC is associated with the reversed north–south density gradient that results from the southward propagation of the perturbation freshwater into the low-latitude North Atlantic. In contrast, the more efficient southward propagation of the temperature anomaly, but less efficient propagation of the salinity anomaly, leads to a smaller density decrease in the low-latitude upper Atlantic and a weaker and less stable RTHC in CM2.1. The rapid salinity recovery over the subtropical North Atlantic in CM2.1 induced by the rapid weakening of the RTHC stimulates large-scale baroclinic eddies, which propagate northward to restart the deep convection in the northern North Atlantic. In addition, the air–sea feedback associated with the southward shift of the Atlantic ITCZ is much more significant in CM2.1, playing an important role in the recovery of the THC.

The difference between R30 and CM2.1 in simulating the stability properties of the THC in the water-hosing experiment is likely an overall result of the different model formulations as shown in Table 1. The different model resolution, numerical schemes, coupling procedure, etc., are among the impact factors. For example, it has been shown that the stability of the THC and RTHC is influenced by the oceanic diapycnal mixing schemes (Manabe and Stouffer 1999; Schmittner and Weaver 2001; Prange et al. 2003; Sijp and England 2006) and the horizontal mixing process (Alley et al. 2003; Longworth et al. 2005; Schlesinger et al. 2006). In addition, the boundary conditions (Ganopolski and Rahmstorf 2001), the representation of air–sea feedbacks (Vellinga et al. 2002; De Vries and Weber 2005), and the Bering Strait Throughflow (Hu and Meehl 2005) could be important in simulating the stability of the THC. The difference in the control climates of R30 and CM2.1 may also contribute to the different sensitivity of the THC to freshwater perturbations.

An additional factor, which we find is important in our analysis of the R30 results, is the use of flux adjustments in this model. As shown by Tables 2 and 3, the simulated net surface water flux over the Atlantic Ocean is very similar between R30 and CM2.1, but this net surface water flux is compensated very differently in R30 and CM2.1. Due to the large flux adjustments employed by R30, the actual net surface water flux felt by the oceanic model is much smaller in R30 than in CM2.1. This leads to a much weaker oceanic freshwater transport and convergence necessary to stabilize the coupled system in R30. In this case, a stable off state of the THC is much more easily obtained. In contrast, the pronounced net surface water flux in CM2.1 has to be totally compensated by oceanic processes only. Therefore, the criteria for a complete freshwater balance in the off state of the THC are much higher. Only the state with an active THC can converge enough freshwater into the Atlantic to offset the subtropical evaporation in CM2.1 (Table 3). The role of the flux adjustments has been investigated in some previous modeling studies, which suggest that the flux adjustments could lead to spurious multiple equilibria of the THC (Dijkstra and Neelin 1999).

CM2.1 represents the current level of the AOGCM development at GFDL. In comparison with R30, CM2.1 employs finer ocean and atmosphere resolution, more up-to-date numerical schemes, and a better coupling procedure without the use of the unphysical virtual salt flux scheme and the use of flux adjustments. Therefore it is likely that the result from CM2.1 is more realistic when applied to the real world, although an important caveat is that both models do not resolve ocean eddies on their respective grids. Studying the impact of ocean eddies on climate will continue to be an important topic in climate research into the future.

Based on the results from both models, we conclude that the RTHC and air–sea feedback are two important features in simulating the stability properties of the THC. The strong tropical air–sea feedback facilitates the recovery of the THC in CM2.1, while a strong development of the RTHC stabilizes the off mode of the THC in R30. As noted earlier, other authors have identified other factors in causing differences in the behavior of the THC. The reader is also reminded that the integrations presented here are transient. One should be cautious when comparing the results with those from the equilibrium runs. Finally, we note that flux adjustments should be used with caution in modeling. Here their use is likely to have impacted the dynamical behavior of the THC in R30.

Acknowledgments. We thank Keith Dixon, Anand Gnanadesikan, Jonathan Gregory, Stephen Griffies, Andrew Weaver, Rong Zhang, and two anonymous reviewers for discussion and suggestions on early versions of this paper. We also thank many others at GFDL for computer and model support.

REFERENCES

Alley, R. B., and Coauthors, 2003: Abrupt climate change. *Science,* **299,** 2005–2010.

Barber, D. C., and Coauthors, 1999: Forcing of the cold event of

8,200 years ago by catastrophic drainage of Laurentide lakes. *Nature,* **400,** 344–348.

Bryan, F., 1986: High-latitude salinity effects and interhemispheric thermohaline circulations. *Nature,* **323,** 301–304.

Bryan, K., 1969: Climate and the ocean circulation. *Mon. Wea. Rev.,* **97,** 806–827.

——, and L. J. Lewis, 1979: A water mass model of the world ocean. *J. Geophys. Res.,* **84,** 2503–2517.

Bryden, H. L., and S. Imawaki, 2001: Ocean heat transport. *Ocean Circulation and Climate: Observing and Modelling the Global Ocean,* G. Siedler et al., Eds., International Geophysical Series, Vol. 77, Academic Press, 455–474.

——, H. R. Longworth, and S. A. Cunningham, 2005: Slowing down of the Atlantic meridional overturning circulation at 25°N. *Nature,* **438,** 655–657.

Chappell, J., 2002: Sea level changes forced ice breakouts in the last glacial cycle: New results from coral terraces. *Quat. Sci. Rev.,* **21,** 1229–1240.

Clarke, G. K. C., D. W. Leverington, J. T. Teller, and A. S. Dyke, 2003: Superlakes, megafloods, and abrupt climate change. *Science,* **301,** 922–923.

Cox, M. D., 1987: Isopycnal diffusion in a *z*-coordinate ocean model. *Ocean Modelling,* **74** (unpublished manuscripts), 1–5.

Cubasch, U., and Coauthors, 2001: Projections of future climate change. *Climate Change 2001: The Scientific Basis,* J. T. Houghton et al., Eds, Cambridge University Press, 525–582.

Delworth, T. L., R. J. Stouffer, K. W. Dixon, M. J. Spelman, T. R. Knutson, A. J. Broccoli, P. J. Kushner, and R. T. Wetherald, 2002: Review of simulations of climate variability and change with the GFDL R30 coupled climate model. *Climate Dyn.,* **19,** 555–574.

——, and Coauthors, 2006: GFDL's CM2 global coupled climate models. Part I: Formulation and simulation characteristics. *J. Climate,* **19,** 643–674.

De Vries, P., and S. L. Weber, 2005: The Atlantic freshwater budget as a diagnostic for the existence of a stable shut down of the meridional overturning circulation. *Geophys. Res. Lett.,* **32,** L09606, doi:10.1029/2004GL021450.

Dijkstra, H. A., and D. J. Neelin, 1999: Imperfections of the thermohaline circulation: Multiple equilibria and flux correction. *J. Climate,* **12,** 1382–1392.

Ganopolski, A., and S. Rahmstorf, 2001: Rapid changes of glacial climate simulated in a coupled climate model. *Nature,* **409,** 153–158.

Gnanadesikan, A., and Coauthors, 2006: GFDL's CM2 global coupled climate models. Part II: The baseline ocean simulation. *J. Climate,* **19,** 675–697.

Gregory, J. M., O. A. Saenko, and A. J. Weaver, 2003: The role of the Atlantic freshwater balance in the hysteresis of the meridional overturning circulation. *Climate Dyn.,* **21,** 707–717.

——, and Coauthors, 2005: A model intercomparison of changes in the Atlantic thermohaline circulation in response to increasing atmospheric CO2 concentration. *Geophys. Res. Lett.,* **32,** L12703, doi:10.1029/2005GL023209.

Griffies, S. M., M. J. Harrison, R. C. Pacanowski, and A. Rosati, 2003: A technical guide to MOM4. NOAA/Geophysical Fluid Dynamics Laboratory Tech. Rep. 5, 295 pp.

——, and Coauthors, 2006: Formulation of an ocean model for global climate simulation. *Ocean Sci.,* **1,** 45–79.

Hu, A., and G. A. Meehl, 2005: Bering Strait throughflow and the thermohaline circulation. *Geophys. Res. Lett.,* **32,** L24610, doi:10.1029/2005GL024424.

Huybrechts, P., and J. de Wolde, 1999: The dynamic response of the Greenland and Antarctic ice sheets to multiple-century climatic warming. *J. Climate,* **12,** 2169–2188.

Lin, S.-J., 2004: A "vertically Lagrangian" finite-volume dynamical core for global models. *Mon. Wea. Rev.,* **132,** 2293–2307.

Lohmann, G., 2003: Atmospheric and oceanic freshwater transport during weak Atlantic overturning circulation. *Tellus,* **55A,** 438–449.

Longworth, H., J. Marotzke, and T. F. Stocker, 2005: Ocean gyres and abrupt change in the thermohaline circulation: A conceptual analysis. *J. Climate,* **18,** 2403–2416.

Manabe, S., and R. J. Stouffer, 1988: Two stable equilibria of a coupled ocean–atmosphere model. *J. Climate,* **1,** 841–866.

——, and ——, 1994: Multiple-century response of a coupled ocean-atmosphere model to an increase of atmospheric carbon dioxide. *J. Climate,* **7,** 5–23.

——, and ——, 1999: Are two modes of thermohaline circulation stable? *Tellus,* **51A,** 400–411.

——, ——, M. J. Spelman, and K. Bryan, 1991: Transient responses of a coupled ocean–atmosphere model to gradual changes of atmospheric CO_2. Part I: Annual mean response. *J. Climate,* **4,** 785–818.

Marotzke, J., and J. Willebrand, 1991: Multiple equilibria of the global thermohaline circulation. *J. Phys. Oceanogr.,* **21,** 1372–1385.

Murray, R. J., 1996: Explicit generation of orthogonal grids for ocean models. *J. Comput. Phys.,* **126,** 251–273.

Pacanowski, R., K. Dixon, and A. Rosati, 1991: The GFDL modular ocean model user guide version 1. GFDL Ocean Group Tech. Rep. 2, 44 pp.

Prange, M., G. Lohmann, and A. Paul, 2003: Influence of vertical mixing on the thermohaline hysteresis: Analyses of an OGCM. *J. Phys. Oceanogr.,* **33,** 1707–1721.

Rahmstorf, S., 1995: Bifurcations of the Atlantic thermohaline circulation in response to changes in the hydrological cycle. *Nature,* **378,** 145–149.

——, 1996: On the freshwater forcing and transport of the Atlantic thermohaline circulation. *Climate Dyn.,* **12,** 799–811.

——, and Coauthors, 2005: Thermohaline circulation hysteresis: A model intercomparison. *Geophys. Res. Lett.,* **32,** L23605, doi:10.1029/2005GL023655.

Rignot, E., and P. Kanagaratnam, 2006: Changes in the velocity structure of the Greenland ice sheet. *Science,* **311,** 986–990.

Saenko, O. A., A. J. Weaver, and J. M. Gregory, 2003: On the link between the two modes of the ocean thermohaline circulation and the formation of global-scale water masses. *J. Climate,* **16,** 2797–2801.

Saltzman, B., 2002: *Dynamical Paleoclimatology: Generalized Theory of Global Climate Change.* International Geophysics Series, Vol. 80, Academic Press, 354 pp.

Schiller, A., U. Mikolajewicz, and R. Voss, 1997: The stability of the thermohaline circulation in a coupled ocean–atmosphere model. *Climate Dyn.,* **13,** 325–348.

Schlesinger, M. E., J. Yin, G. Yohe, N. G. Andronova, S. Malyshev, and B. Li, 2006: Assessing the risk of a collapse of the Atlantic thermohaline circulation. *Avoiding Dangerous Climate Change,* J. Schellnhuber et al., Eds., Cambridge University Press, 392 pp.

Schmittner, A., and A. J. Weaver, 2001: Dependence of multiple climate states on ocean mixing parameters. *Geophys. Res. Lett.,* **28,** 1027–1030.

Sijp, W. P., and M. H. England, 2006: Sensitivity of the Atlantic thermohaline circulation and its stability to basin-scale variations in vertical mixing. *J. Climate,* **19,** 5467–5478.

Stocker, T. F., and D. G. Wright, 1991: Rapid transitions of the ocean's deep circulation induced by changes in the surface water fluxes. *Nature,* **351,** 729–732.

——, and A. Schmittner, 1997: Rate of global warming determines the stability of the ocean-atmosphere system. *Nature,* **388,** 862–865.

Stommel, H. M., 1961: Thermohaline convection with two stable regimes of flow. *Tellus,* **13,** 224–230.

Stouffer, R. J., and Coauthors, 2006a: Investigating the causes of the response of the thermohaline circulation to past and future climate changes. *J. Climate,* **19,** 1365–1387.

——, and Coauthors, 2006b: GFDL's CM2 global coupled climate models. Part IV: Idealized climate response. *J. Climate,* **19,** 723–740.

Talley, L. D., 1996: Antarctic intermediate water in the South Atlantic. *The South Atlantic: Present and Past Circulation,* G. Wefer et al., Eds., Springer, 219–238.

Tziperman, E., 1997: Inherently unstable climate behaviour due to weak thermohaline ocean circulation. *Nature,* **386,** 592–595.

Vellinga, M., R. A. Wood, and J. M. Gregory, 2002: Processes governing the recovery of a perturbed thermohaline circulation in HadCM3. *J. Climate,* **15,** 764–780.

Weaver, A. J., and T. M. C. Hughes, 1994: Rapid interglacial climate fluctuations driven by North Atlantic Ocean circulation. *Nature,* **367,** 447–450.

Wittenberg, A. T., A. Rosati, N.-C. Lau, and J. J. Ploshay, 2006: GFDL's CM2 global coupled climate models. Part III: Tropical Pacific climate and ENSO. *J. Climate,* **19,** 698–722.

Wunsch, C., 2002: What is the thermohaline circulation? *Science,* **298,** 1179–1181.